

SHORT REPORT

Innovative Tools and Methods

Clonal expansion of intra-epithelial T cells in breast cancer revealed by spatial transcriptomics

Lou Romanens¹  | Prasad Chaskar^{1,2} | Rachel Marccone³  | Stephan Ryser¹ | Jean-Christophe Tille⁴  | Raphael Genolet⁵ | Ketty Heimgartner-Hu¹ | Killian Heimgartner¹ | Jonathan S. Moore¹ | Nicolas Liaudet⁶  | Gürkan Kaya^{4,7} | Mikael J. Pittet^{2,8,9,10} | Pierre-Yves Dietrich^{1,2}  | Mauro Delorenzi^{3,5}  | Daniel E. Speiser⁵ | Alexandre Harari^{5,10} | Petros Tsantoulis^{1,2}  | Sana Intidhar Labidi-Galy^{1,2} 

¹Faculty of Medicine, Department of Medicine and Center of Translational Research in Onco-Hematology, University of Geneva, Swiss Cancer Center Leman, Genève, Switzerland

²Department of Oncology, Hôpitaux Universitaires de Genève, Genève, Switzerland

³SIB Swiss Institute of Bioinformatics, Lausanne, Switzerland

⁴Department of Diagnosis, Division of Clinical Pathology, Hôpitaux Universitaires de Genève, Genève, Switzerland

⁵Department of Oncology UNIL CHUV, Ludwig Institute for Cancer Research, University of Lausanne, Swiss Cancer Center Leman, Lausanne, Switzerland

⁶Bioimaging Core Facility, Faculty of Medicine, University of Geneva, Genève, Switzerland

⁷Department of Medicine, Division of Dermatology, Hôpitaux Universitaires de Genève, Genève, Switzerland

⁸Department of Pathology and Immunology, Faculty of Medicine, University of Geneva, Genève, Switzerland

⁹Ludwig Institute for Cancer Research, Lausanne, Switzerland

¹⁰AGORA Cancer Center, Lausanne, Switzerland

Correspondence

Petros Tsantoulis and Sana Intidhar Labidi-Galy, Department of Oncology, Hôpitaux Universitaires de Genève, Rue Gabrielle Perret-Gentil 4, 1204, Geneva, Switzerland. Email: petros.tsantoulis@hcuge.ch and intidhar.labidi-galy@hcuge.ch

Funding information

Fonds De La Recherche Scientifique-FNRS, Grant/Award Number: PZ00P3_173959

Abstract

The spatial distribution of tumor-infiltrating lymphocytes (TIL) predicts breast cancer outcome and response to systemic therapy, highlighting the importance of an intact tissue structure for characterizing tumors. Here, we present ST-FFPE, a spatial transcriptomics method for the analysis of formalin-fixed paraffin-embedded samples, which opens the possibility of interrogating archival tissue. The method involves extraction, exome capture and sequencing of RNA from different tumor compartments microdissected by laser-capture, and can be used to study the cellular composition of tumor microenvironment. Focusing on triple-negative breast cancer (TNBC), we characterized

Abbreviations: AEC, aminoethyl carbazole; BCR, B-cell receptor; CAF, cancer-associated fibroblasts; cDNA, complementary deoxyribonucleic acid; cTIL, core tumor-infiltrating lymphocytes; DEPC, diethyl pyrocarbonate; ecRNA-seq, exome-capture RNA-sequencing; EtOH, ethanol; Fab, fragment antigen-binding; FC, fold change; FDA, food and drug administration; FDR, false discovery rate; FF, fresh-frozen; FFPE, formalin-fixed paraffin-embedded; Fib, fibroblasts; GSVA, gene set variation analysis; H&E, hematoxylin and eosin; IHC, immunohistochemistry; IVT, in vitro transcription; LCM, laser-capture microdissection; MCP-counter, microenvironment cell population counter; NK, natural killer cells; PC1/2, principal component 1/2; PCA, principal component analysis; PCR, polymerase chain reaction; PET, polyethylene terephthalate; qRT-PCR, quantitative real-time polymerase chain reaction; RIN, RNA integrity number; RNA, ribonucleic acid; RNA-seq, RNA-sequencing; ST, spatial transcriptomics; sTIL, stromal tumor-infiltrating lymphocytes; TC, tumor core; TCR, T-cell receptor; TIL, tumor-infiltrating lymphocytes; TNBC, triple-negative breast cancer; UV, ultra-violet.

This is an open access article under the terms of the [Creative Commons Attribution](https://creativecommons.org/licenses/by/4.0/) License, which permits use, distribution and reproduction in any medium, provided the original work is properly cited.

© 2023 The Authors. *International Journal of Cancer* published by John Wiley & Sons Ltd on behalf of UICC.

T cells, B cells, dendritic cells, fibroblasts and endothelial cells in both stromal and intra-epithelial compartments. We found a highly variable spatial distribution of immune cell subsets among tumors. This analysis revealed that the immune repertoires of intra-epithelial T and B cells were consistently less diverse and more clonal than those of stromal T and B cells. T-cell receptor (TCR) sequencing confirmed a reduced diversity and higher clonality of intra-epithelial T cells relative to the corresponding stromal T cells. Analysis of the top 10 dominant clonotypes in the two compartments showed a majority of shared but also some unique clonotypes both in stromal and intra-epithelial T cells. Hyperexpanded clonotypes were more abundant among intra-epithelial than stromal T cells. These findings validate the ST-FFPE method and suggest an accumulation of antigen-specific T cells within tumor core. Because ST-FFPE is applicable for analysis of previously collected tissue samples, it could be useful for rapid assessment of intratumoral cellular heterogeneity in multiple disease and treatment settings.

KEYWORDS

clonal expansion, laser-capture microdissection, spatial TCR, spatial transcriptomics, TCR-sequencing

Whats new?

The abundance and spatial distribution of tumor-infiltrating lymphocytes (TIL) in breast cancer tumors correlates with outcome. Here, the authors demonstrated the feasibility of a spatial transcriptomics method to analyze formalin-fixed paraffin-embedded tissue samples, or ST-FFPE, in triple-negative breast cancer. Using this method, they observed the cellular composition of the tumor microenvironment and found that intra-epithelial TIL showed reduced diversity and increased clonality compared with stromal TIL. In addition to studying TIL populations, the method could have clinical usefulness for predicting response to immunotherapy.

1 | INTRODUCTION

Solid tumors are composed of cancer cells and non-cancer cells such as immune cells, fibroblasts and endothelial cells,^{1,2} whose proportions and state vary from tumor to tumor. The abundance of tumor-infiltrating lymphocytes (TIL) correlates with a better outcome in various cancers. Importantly, the prognostic and predictive value of TIL depends on their spatial localization.³ In breast cancer, TIL that are located in the stroma between cancer cells and do not directly contact cancer cells, namely stromal TIL (sTIL), have a prognostic value.⁴ Assessment of the abundance of sTIL by hematoxylin and eosin (H&E) staining is now implemented in routine clinical practice.⁵ In contrast, in other cancers such as melanoma, it is the presence of intra-epithelial CD8⁺ T cells, that is, lymphocytes located in tumor core (cTIL) and directly interacting with cancer cells with no intervening stroma, that has prognostic value⁶ and is predictive of response to PD-1 blockade,⁷ highlighting the importance of spatial analysis of tumor immune microenvironment.

Stromal and intra-epithelial TIL can be highly heterogeneous in terms of composition, phenotype and antigen specificity. Notably, a substantial proportion of TIL are bystander T cells, which are specific to diverse epitopes unrelated to tumor antigens such as viral antigens.⁸⁻¹⁰ Hence, it is important to assess the tumor antigen-specificity of T cells, since successful cancer immunotherapy requires their reactivation and clonal expansion of tumor-reactive T cells.^{11,12} Because

antigen specificity comes from T-cell receptors (TCR), TCR repertoires are actively characterized in order to identify tumor-reactive T cells. For instance, the increased prevalence of TIL sharing the same TCR correlates with a better response to cancer immunotherapy,¹³⁻¹⁵ suggesting that these TIL include T cells reactive to tumor antigens.

Laser-capture microdissection (LCM) is a suitable tool for studying spatially distinct regions of interest such as tumor core and adjacent stroma.¹⁶⁻¹⁸ Here, we developed ST-FFPE, a robust spatial transcriptomics method that combines LCM with RNA extraction, exome-capture and sequencing, and can be used for the analysis of formalin-fixed paraffin-embedded (FFPE) tumor samples. We demonstrate the relevance of this approach by investigating the spatial distribution of clonally expanded T cells localized within tumors from TNBC patients. Our method can elucidate intratumoral immune cell dynamics with potential implications for cancer immunotherapy.

2 | MATERIALS AND METHODS

2.1 | Samples and inclusion criteria

FFPE and fresh-frozen (FF) samples of TNBC patients were provided by the division of clinical pathology, Hôpitaux Universitaires de Genève. All tumor sections were reviewed by a board-certified pathologist (J.C.T.).

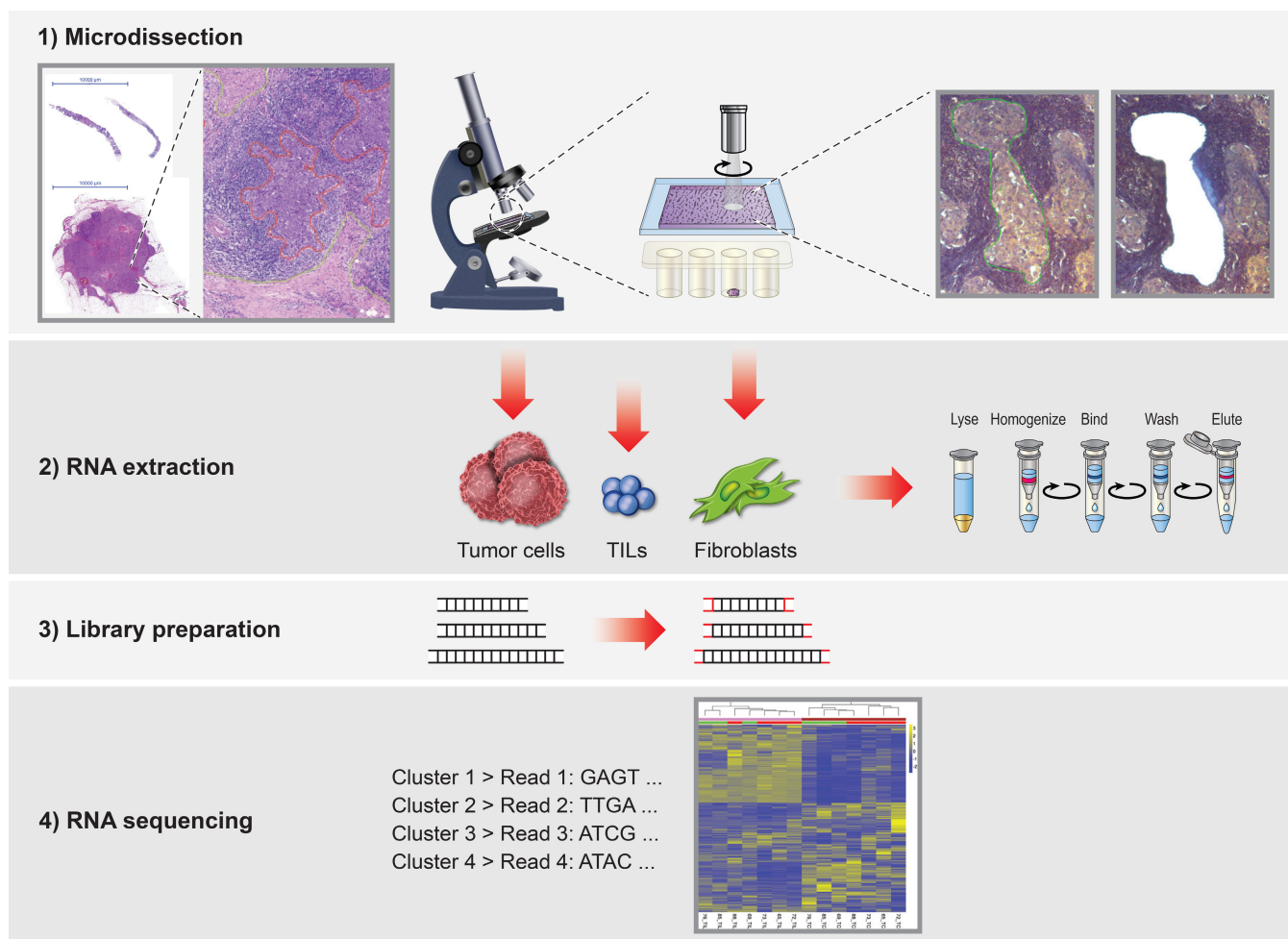


FIGURE 1 Workflow of laser capture microdissection and RNA-sequencing. Step 1: TNBC (core needle or surgical biopsies) tissue sections mounted on PET slides are stained with hematoxylin and submitted to laser-capture microdissection (LCM) to collect separately tumor core (TC), stromal tumor-infiltrating lymphocytes (sTIL) and fibroblasts (Fib) under direct microscopic visualization. Cells of interest are selected using the Laser Microdissection device software. Selected regions of interest are cut from tumor sections with a laser beam and collected within the cap of a PCR tube placed under the PET slide. Step 2: RNA extraction from microdissected TC, sTIL and Fib. Step 3: library preparation including the conversion of RNA into cDNA fragments and the addition of adaptors. Step 4: libraries are subjected to exome-capture RNA-sequencing.

2.2 | Laser capture microdissection of FFPE tissue

Polyethylene terephthalate (PET) slides were pretreated by coating with 300 μ l poly-lysine (Sigma-Aldrich, St-Louis, United States) and exposure to UV for 30 min. Consecutive sections from FFPE blocks were cut at 8 μ m, floated onto a 45°C water bath and mounted on PET slides. After drying in a slide holder for 30 min at room temperature, tissue sections were dewaxed in xylene, rehydrated with decreasing concentrations of ethanol, stained with hematoxylin, dehydrated with increasing concentrations of ethanol, and cleared in xylene (Detailed timing and concentrations in Table S1 and Section 3). Eight protocols were tested and the optimal protocol was b: briefly, deparaffinization was performed in fresh xylene for 1 min twice followed by 100% ethanol for 1 min, 95% for ethanol 1 min and 75% ethanol for 1 min. The slides were transferred into diethyl pyrocarbonate (DEPC) water for 2 min before staining with hematoxylin for 2 min. Subsequently, slides were rinsed in DEPC water until they became clear before undergoing dehydration in 75% ethanol

for 1 min, 95% ethanol for 1 min, 100% ethanol for 2 min and xylene for 1 min.

A minimal surface of 2.5 mm² of tumor core (TC), fibroblasts (Fib) and sTIL was microdissected using the Laser Microdissection Systems LMD7000 with the laser parameters (laser power of 39 mW, a wavelength of 349 nm, pulse frequency of 664 Hz and pulse energy of 120 μ J) and collected separately in RNase-free tube. For each microdissected block, a consecutive 4 μ m thick tissue section was stained with H&E to help recognize tissue's morphology under the LMD7000 microscope (Figure 1).

2.3 | RNA extraction, quantification and fragment size analysis

For microdissected FF cells, RNA was extracted using RNeasy Plus Micro Kit (Qiagen, Hilden, Germany) according to the supplier's

protocol. Microdissected cells from FFPE tissue were lysed by incubation with proteinase K at 56°C while stirring at 400 rpm for 3 h. RNA was extracted using RNeasy FFPE kit (Qiagen, Hilden, Germany) according to the supplier's protocol, treated with DNase I, eluted in 15 µl of RNase-free water and stored at -80°C. Total RNA was quantified using Qubit RNA HS Assay Kit and Qubit Fluorometer (Thermo Fisher Scientific, MA). RNA fragment size was analyzed with the 2100 Bioanalyzer (Agilent, CA) using Eukaryote total RNA Pico assay (Agilent, CA, USA). In case of insufficient RNA concentration, samples were concentrated using a Vacuum Concentrator Centrifuge (UNIVAPO 100 ECH, Uniequip, Germany) to reach the minimum volume recommended by the TruSeq RNA Exome kit.

Supplementary methods are available online.

3 | RESULTS

3.1 | Workflow of FFPE laser capture microdissection and exome-capture RNA-sequencing

Our procedure of ST-FFPE involved the following steps: laser microdissection of regions of interest (step 1), RNA-extraction (step 2), library preparation including the conversion of RNA into cDNA fragments (step 3) and exome-capture RNA-sequencing (step 4) (Figure 1). The regions of interest were tumor core (TC), sTIL and fibroblasts (Fib) (Figure S1).

We first optimized the tissue preparation process before LCM on three TNBC blocks. We aimed to shorten the H&E staining procedure in order to reduce further degradation of nucleic acids,¹⁹ while conserving maximal morphological contrast between cell subtypes. Thus, we tested eight different protocols (a-h) previously described for LCM procedures²⁰⁻²² with three different dyes (hematoxylin, eosin and cresyl violet) and varying durations of incubation in xylene and ethanol (Figure S1). The optimal staining was obtained with protocol b (see methods) that allowed the best morphological distinction between the three cell subsets (sTIL, TC and Fib; Figure S2) while having the shortest exposure to xylene that partially degrades RNA.¹⁹

Second, we aimed to optimize RNA extraction from FFPE samples in view of subsequent RNA-sequencing (RNA-seq), for which we had to choose the most appropriate protocol. In highly degraded and small amounts of RNA, RNA-seq via poly(A) selection does not perform well because poly(A) tail can be lost.²³ Exome-capture protocol has been previously shown to perform better than ribosomal RNA depletion,²³ with minimal differences when comparing FFPE and matched FF samples.^{24,25} Thus, we chose this approach. The minimal requirements for exome-capture RNA-sequencing (ecRNA-seq) with the TruSeq protocol are: (a) RNA integrity number (RIN) > 1.4, (b) a percentage of fragments over 200 nucleotides (DV_{200}) > 30% and (c) a minimum yield of 40 to 55 ng depending on RNA's quality.

Extracting RNA from 2 mm² microdissected area of TC using manufacturer's protocol (eg, elution volume of 30 µl) resulted in an undetectable yield (Figure S3A). Therefore, we introduced several modifications to this protocol, by reducing the eluted volume to 15 µl, adding

mechanical digestion by stirring (400 rpm) and concentrating the volume using a vacuum concentrator centrifuge to reach a final volume of 4 µl. This optimized protocol rendered RNA detectable (yield of 18-40 ng). Next, we tested four different durations (15 min, 1 h, 3 h and overnight) of enzymatic digestion with proteinase K. RNA yield tended to increase with prolonged digestion, whereas RIN was not affected and DV_{200} initially reached a maximum at 3 h but declined after overnight digestion (Figure S3B-D). Thus, 3 h was set as the optimal duration of tissue digestion. These modifications led to the final protocol (Figure S3E).

3.2 | Transcriptomes of microdissected FFPE tissues are concordant with matched cryopreserved tissues

We examined the performance and reproducibility of ecRNA-seq with the TruSeq protocol for gene expression profiling of microdissected TC (~20 mm²) processed as described above for FFPE, and matched fresh frozen (FF) sections as described previously,²⁶ obtained from three TNBC patients and stored over 5 to 9 years (Figure S4 and Table S2). On average, we obtained 63.8 million reads per sample for FFPE RNA, while the yield was 134.2 million reads per sample for FF RNA. We performed quality control of raw sequencing reads using the FastQC tool. All samples passed the per base and per sequence quality score criteria with a mean Phred quality score of ~40. After alignment to the human reference transcriptome (GRCh38 cDNA), we obtained an average mapping rates of 83.0% for FFPE RNA and 91.8% for FF RNA. Transcriptomics of microdissected TC from matched FFPE and FF cases showed a correlation over 90% (Figure S5A-C and Figure 2A), suggesting that ecRNA-seq allows concordant transcriptomic analysis between FF and FFPE samples.

3.3 | Transcriptomes of spatially distinct compartments are consistent with the morphology of microdissected cells

We applied our optimized protocol of LCM and RNA extraction to distinct compartments (TC, sTIL and Fib) of seven FFPE TNBC blocks (2 core needle biopsies and five surgical biopsies) aged from 3 to 10 years. Sufficient RNA for subsequent sequencing was collected from all microdissected TC and sTIL samples. With a theoretical expected RNA amount of 20 pg/cell, the performance of RNA extraction was estimated to 15% for TC and 8% for sTIL. Sufficient RNA extraction from microdissected Fib was successful in only two out of seven tumors (Figure 2B). The age of the block did not impact RNA yield or RIN (Figure 2C, D) but we noticed a downwards trend of DV_{200} level in older blocks (Figure 2E). In the end, we could perform ecRNA-seq on 16 samples (7 TC, 7 sTIL, 2 Fib, Table S3). ecRNA-seq was performed in multiplex, yielding an average of 98.7 million paired-end stranded reads, and all samples passed the per base and per sequence quality score criteria (Table S4). On average, 76% of reads successfully aligned with the reference transcriptome.

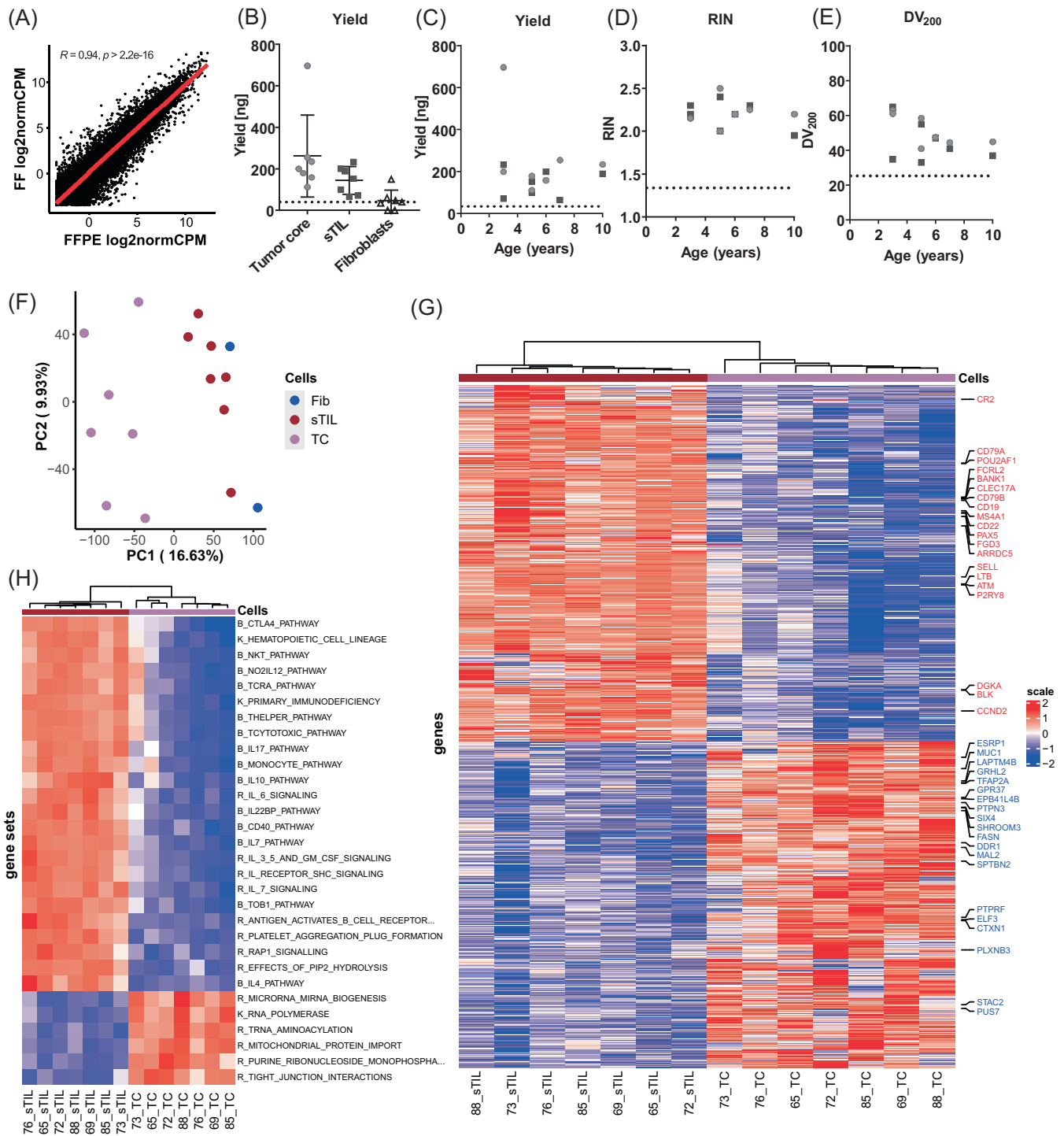


FIGURE 2 Differential gene expression of microdissected tumor core and stromal TIL from FFPE TNBC. (A) Correlation between merged FFPE transcriptomes and merged FF transcriptomes of microdissected TC from three TNBC samples. (B) Yield of RNA collected from microdissected TC, sTIL and Fib from seven FFPE samples of TNBC. (C-E) RNA yield, DV₂₀₀ and RIN of RNA extracted from microdissected sTIL and TC, according to the age of FFPE blocks. Dashed lines represent the minimal RNA quantity and quality required for subsequent RNA-sequencing. (F) Principal component analysis PCA of microdissected TC (n = 7), sTIL (n = 7) and Fib (n = 2) from seven TNBC samples where each dot indicates a sample. (G) Heatmap based on the hierarchical clustering of seven TC (in brown) and seven sTIL (in pink). (H) Heatmap based on Gene Set Variant Analysis, pathways enriched in TC and sTIL. Color scale: red, high relative expression; blue, low relative expression. B, Bioconductor; DV₂₀₀, percentage of RNA fragments >200 nucleotides; FF, fresh-frozen; FFPE, formalin-fixed paraffin-embedded; Fib, fibroblasts; K, KEGG; PC, principal component; R, Reactome; RIN, RNA integrity number; sTIL, stromal tumor-infiltrating lymphocytes; TC, tumor core.

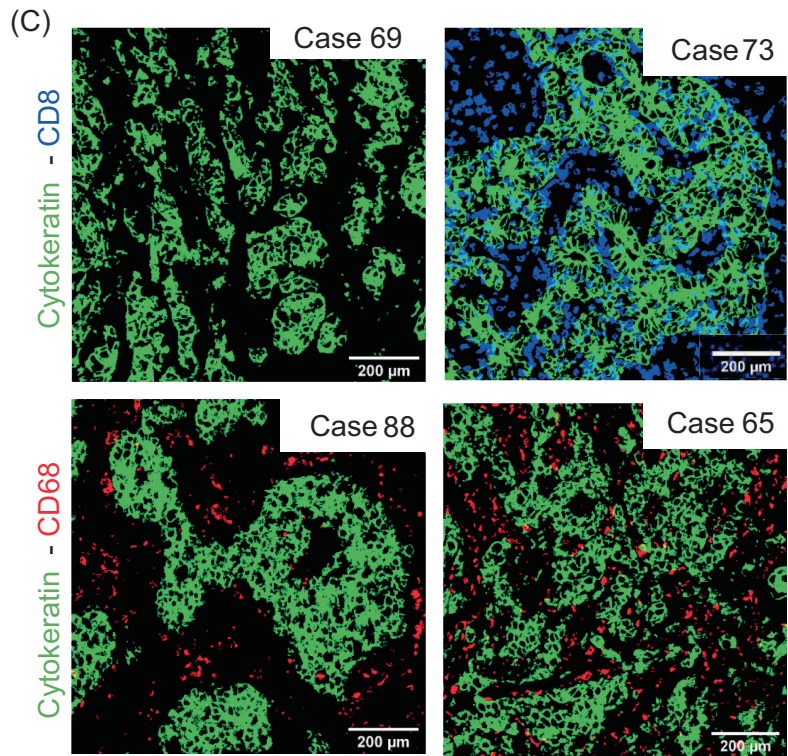
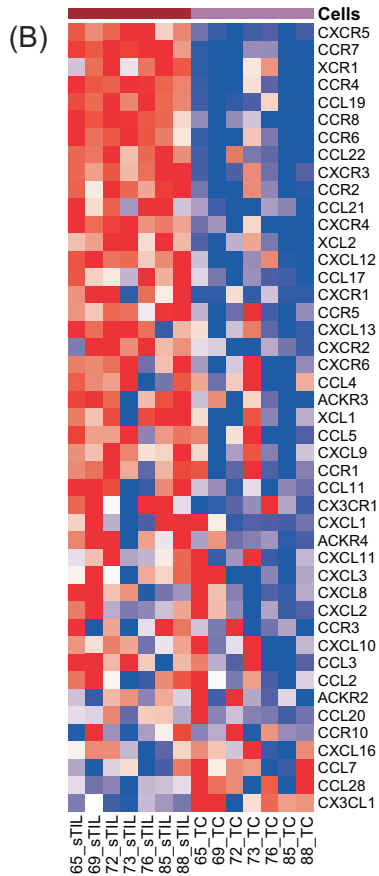
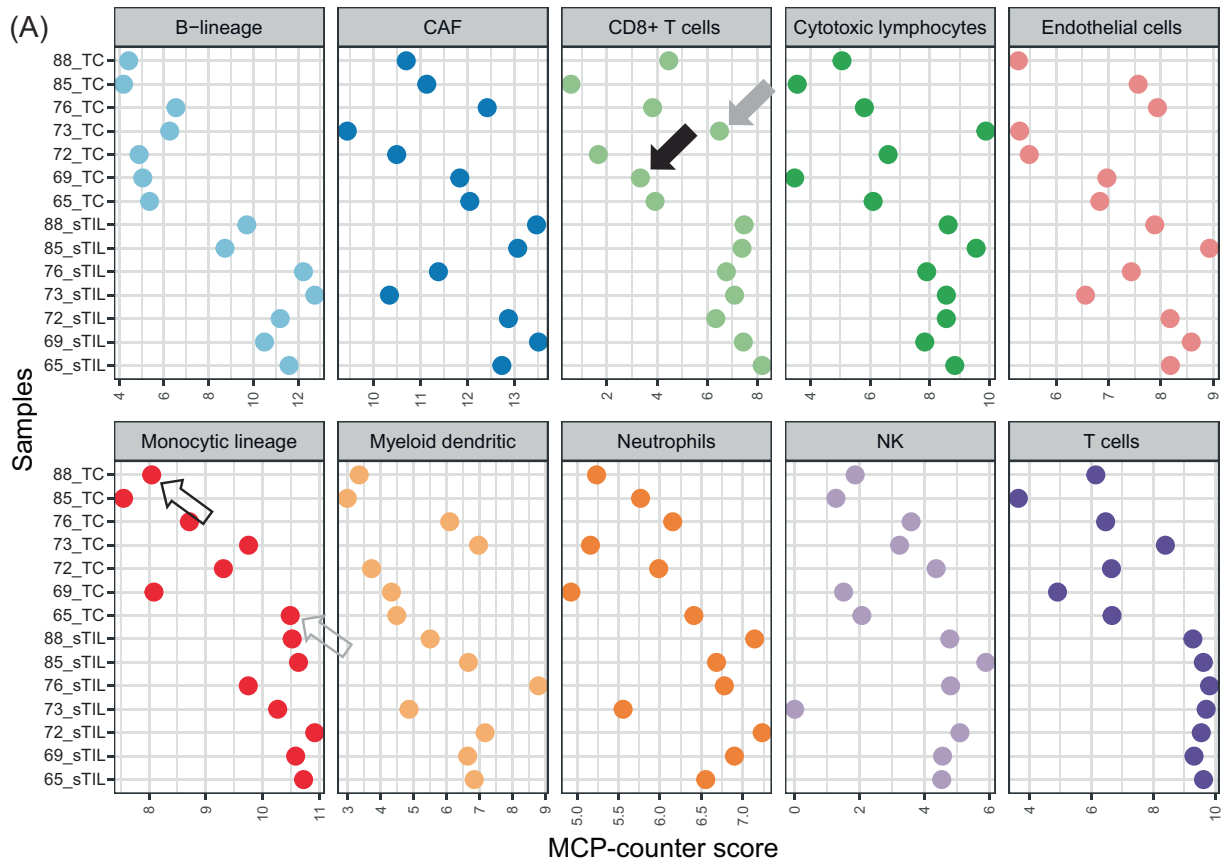


FIGURE 3 Legend on next page.

Principal Component Analysis (PCA) was performed based on the variance stabilized gene count matrix. A scatter plot of PC1 and PC2 displays separated TC, sTIL and Fib (Figure 2F). Overall, PCA showed that TC samples are more similar to each other than they are to sTIL and Fib. The same holds true for sTIL and Fib samples. The number of Fib samples ($n = 2$) was not sufficient for statistical analysis, and they were excluded from further analyses. PCA and hierarchical clustering based on correlation distance (Figure 2H) confirmed that the different cell populations, microdissected based on their distinct morphology, are also transcriptionally different as expected.

GSVA analyses revealed the enrichment of several canonical pathways related to immune cell functions such as TCR signaling, NKT signaling, BCR signaling, JAK-STAT signaling and IL-2/3/5 signaling in sTIL. Pathways related to cell cycle, cell junction organization, membrane trafficking were also significantly enriched in TC (Figure 2G). We identified 1616 genes that were differentially expressed between TC and sTIL (898 genes upregulated in sTIL and 718 genes upregulated in TC) (Tables S5 and S6). Differential expression analyses identified *MUC1* among the most significantly upregulated genes in TC. *MUC1* (CA15-3) is a well-characterized transmembrane mucin upregulated by 90% of TNBC²⁷ and it is an FDA-approved serum tumor marker for monitoring metastatic breast cancer. In addition, TC expressed several epithelial markers like *EPCAM*, *KRT8*, *KRT18* and *KRT19*.

Among top upregulated genes in sTIL, we noted several markers of B-cells (*CD79A*, *CD79B*, *PAX5*, *BLNK* and *MS4A1*) and T cells (*CD2*, *CD3D*, *CD3E*, *CD3G* and *CD8B*) (Table S5). Overall, the identification of immune cell-specific transcriptional profiles in microdissected sTIL and epithelial markers in microdissected TC further validate our spatial selection.

We used quantitative RT-PCR (qRT-PCR) to assess the expression of genes to identify those that are significantly upregulated in TC vs sTIL and sTIL vs TC. Ten genes were evaluated: five genes upregulated in sTIL (*CD28*, *CCR7*, *CD79B*, *FCMR* and *PAX5*) and five genes upregulated in TC (*ELF3*, *MAL2*, *MUC1*, *TFAP2A* and *GPR37*) (Table S7). The qRT-PCR results confirmed our RNA-sequencing data (Figure S6A,B).

3.4 | Spatial distribution of immune cell subsets in distinct tumor compartments revealed through deconvolution with MCP-counter

We estimated the abundance of immune cell subpopulations in both TC and sTIL compartments by deconvoluting RNAseq data with Microenvironment Cell Population (MCP)-counter.²⁸ The spatial distribution of

immune cells was variable across the seven cases of TNBC. For instance, CD8⁺ T-cell abundance estimate was high in microdissected TC from case 73 (full gray arrow, Figure 3A) and low in case 69 (full black arrow, Figure 3A), consistent with the up-regulation of T-cell chemoattractive chemokines *CCR5* and *CXCL9* in case 73 and their downregulation in case 69 (Figure 3B). Multiplexed IHC confirmed massive intraepithelial accumulation of CD8⁺ cells in case 73, and their absence in case 69 (Figure 3C) where they were rather present at tumor margins. High spatial variability was also observed in the monocytic lineage. For instance, the monocyte abundance estimate was high in microdissected TC from case 65 (empty gray arrow, Figure 3A) and low in case 88 (empty black arrow, Figure 3A). Multiplexed IHC confirmed the accumulation of intraepithelial CD68⁺ cells in this case, whereas they were mainly in the stromal compartment surrounding TC in case 88 (Figure 3C). Overall, the spatial distribution of immune cell subsets by transcriptomics was concordant with multiplexed IHC.

3.5 | Spatial transcriptomics revealed clonal expansion of intra-epithelial T cells as compared with matched stromal T cells

We took advantage of the high potential of the spatial transcriptomics method to address biologically relevant questions and investigate the immune repertoires of intra-epithelial T and B cells, that is, located in TC (cTIL), and matched stromal T and B cells (sTIL). Interestingly, the immune repertoires of cTIL were systematically less diverse than sTIL in the seven TNBC cases ($P = .02$, paired Wilcoxon test; Figure 4A), while their clonality was higher in six out of seven cases ($P = .03125$, paired wilcoxon test, Figure S7). In order to further study the diversity and clonality of T-cell receptor (TCR) repertoire of intra-epithelial and matched stromal T cells, we performed TCR-sequencing²⁹ on microdissected TC (that contains cTIL) and sTIL from seven fresh frozen TNBC samples (Table S8). Diversity was reduced in cTIL as compared with matched sTIL in six out of seven cases (two-tailed paired *T* test $P = .008$; Figure 4B). Conversely, clonality of cTIL repertoires was consistently higher (two-tailed paired *T* test $P = .021$; Figure 4C), and tumor core samples harbored a higher fraction of hyperexpanded clonotypes compared with matched stromal samples ($P = .005$; Figure 4D). Next, we evaluated the overlap between cTIL and sTIL TCR-repertoires. In six out of seven patients, the cumulative frequency of shared clonotypes (ie, their relative contribution in each repertoires) was higher in cTIL as compared with sTIL (Figure 4E), consistent with the higher clonality of cTIL TCR repertoire. We next

FIGURE 3 Abundance of immune cell sub-populations in tumor core and stromal TIL estimated with MCP-counter. (A) Dot-charts of eight immune cell subpopulations, cancer-associated fibroblasts (CAF) and endothelial cells estimated by MCP-counter in paired microdissected TC and sTIL ($n = 7$). Gray empty arrow (case 69) and black empty arrow (case 88) indicate TC samples that are enriched or poor in monocytic cells, respectively. Gray full arrow (case 73) and black full arrow (case 69) indicate TC samples that are enriched or poor in CD8⁺ T cells, respectively. (B) Heatmaps of chemokines in microdissected sTIL (pink) and TC (brown). (C) Representative multiplex IHC images showing the presence (case 65) or absence (case 88) of intra-epithelial CD68⁺ monocytic cells. Multiplex IHC showed the presence (case 73) or absence (case 69) of intra-epithelial CD8⁺ T cells. Epithelial cells are Cytokeratin⁺. CAF: cancer associated fibroblasts. NK, Natural Killer lymphocytes; sTIL, stromal tumor-infiltrating lymphocytes; TC = tumor core.

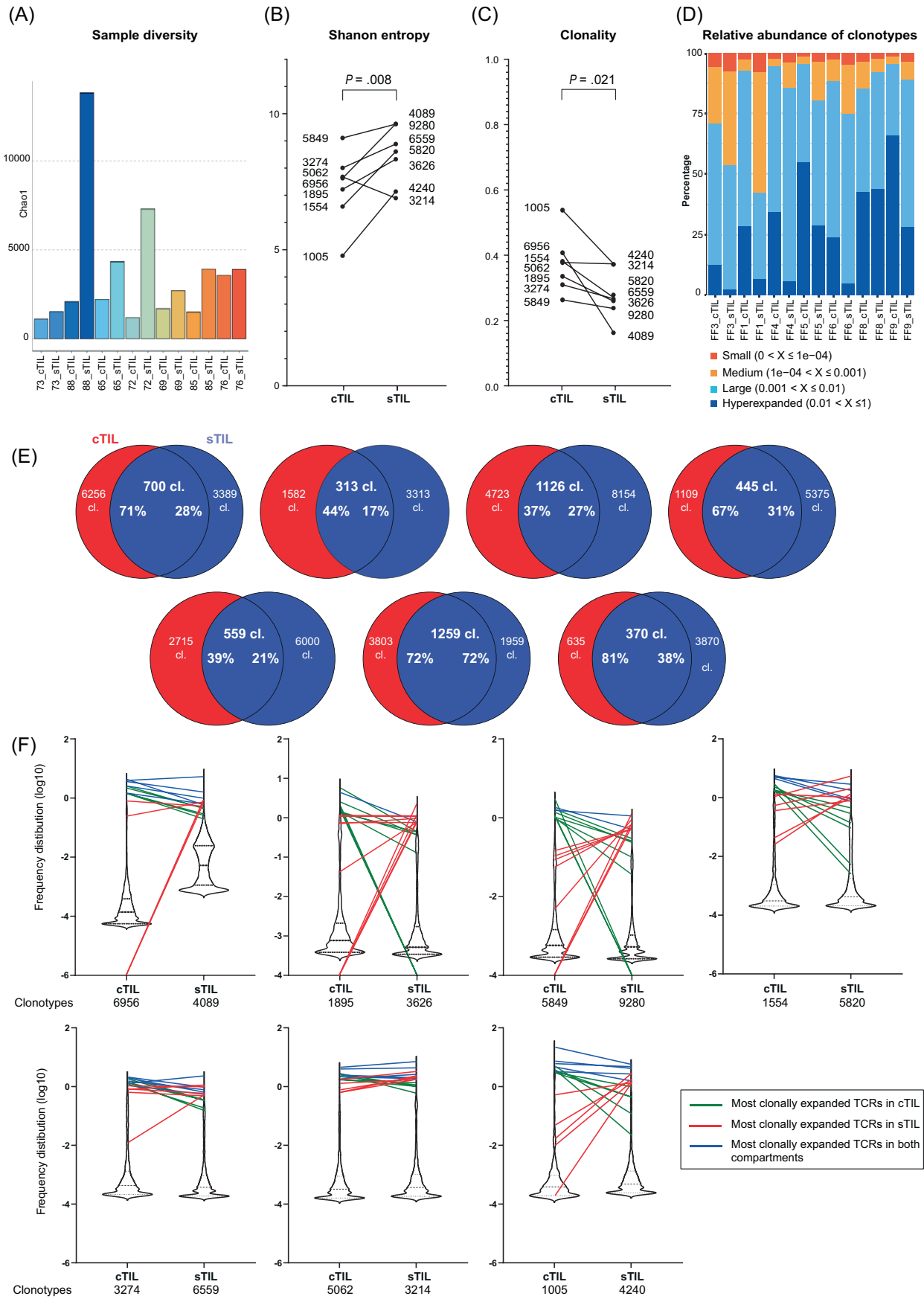


FIGURE 4 Legend on next page.

investigated the contribution of the most abundant clonotypes to TCR-repertoire differences between cTIL and sTIL. Analysis of the top 10 dominant clonotypes of each cTIL and sTIL repertoires showed a majority of shared but also some unique clonotypes (Figure 4F) both in cTIL and sTIL. Together, these findings highlight a different clonotypic composition of sTIL vs cTIL, and an increased clonal expansion of intra-epithelial T cells, potentially due to specific tumor antigen recognition. When comparing TCR repertoires from cTIL or sTIL to those of bulk samples (Figure S8), we noticed that both diversity and clonality of bulk TCR repertoire were mainly driven by sTIL TCR repertoire (diversity and clonality of bulk vs sTIL: $P = .45$ and $P = .94$, respectively) and differed from intra-epithelial TCR diversity (diversity and clonality of bulk vs TC: $P = .06$ and $P = .15$, respectively). This observation suggests that characterization of intra-epithelial TIL, which are of interest for anti-tumor response, is not tangible in bulk tumor samples analysis, highlighting the relevance of spatial characterization.

4 | DISCUSSION

In summary, we demonstrated the feasibility of using our method for spatial transcriptomic analysis of archived FFPE samples from TNBC patients. We exploited the potential of this method and reported an increased clonality and reduced diversity of the immune repertoire of intra-epithelial TIL, compared with stromal TIL. Due to the reduced sensitivity of analyzing immune repertoire from bulk RNA-sequencing of FFPE tissue (on average ~ 350 TCR clones could be analyzed) resulting from the limited depth of sequencing of TCR/BCR and the need of 150 bp to identify a TCR (V, CDR3 and J regions), we performed TCR-sequencing of microdissected FF samples allowing a wider assessment of TCR clones (on average $\sim 10,000$ clones). With such approach, we were able to confirm a reduced diversity of intra-epithelial TIL, and their clonal expansion as compared with matched stromal ones. This finding is of great interest, as an increased clonal expansion suggests specificity for tumor antigens, and tumor-reactive T cells in direct contact with cancer cells are more likely to mediate clinical benefit of immunotherapy. We consistently observed (ie, in six out of the seven regions analyzed) higher clonality in tumors as compared with cognate stroma. Interpretations of changes in tumor repertoires (between different regions or timepoints etc.) are always limited by the concern of tumor heterogeneity, as well as undersampling. As the tumor regions were randomly selected, we can assume that even

though the clonality of the tumor may vary from one region to the other, it is more clonal than the adjacent stromal part.

The importance of clonal expansion of intra-epithelial TIL is relevant for a variety of reasons: (i) pathologists cannot reliably assess intra-epithelial TILs, that is why an international consortium, the TILs-WG (www.tilsinbreastcancer.org)⁵ formally states that only stromal TILs should be assessed in a reproducible manner by breast cancer pathologists, and this is particularly true for TNBC^{4,30}; (ii) it is increasingly evident that an increase of intra-epithelial TILs are probably an expansion of so-called tissue resident (memory) CD8⁺ T cells, which are enriched within cancer islands.^{31,32} Conceptually, these intra-epithelial TILs have always been there (meaning that not all immigrate from the systemic circulation) and are likely tumor antigen-specific, promoting a favorable clinical outcome.^{33,34} While the milder association with anti-tumor effects, and the high diversity/low clonality of the TCR repertoire of stromal TILs suggest that they are partly “bystander” populations coming from the systemic circulation.³⁵ Considering the proven clinical importance of stromal TILs,³⁶ it may be envisaged that both compartments should be analyzed in order to understand the immune-system of our patients. Such spatial characterization could also be extent to lymph nodes, given their increasingly importance in the context of breast cancer.³⁷

Our study has also clinical implications. Although anti-PD1 blockade prolongs the survival of TNBC patients,^{38,39} a significant proportion of them does not benefit from immunotherapy. Spatial profiling could be incorporated in clinical trials and daily practices. Here, we propose to first assess the abundance of stromal TILs on H&E sections, as this is an unexpensive and well-implemented approach in clinical pathology. Given the absence of reliable predictive biomarkers for response to PD1-blockade in TNBC, spatial profiling could be used for patients that have the same amount of stromal TILs but different outcome or response to PD1-blockade, to understand the biological mechanisms driving response to immunotherapy. Thus, a complementarity approach between pathologists and molecular biologists in the clinics would help developing precision immunotherapy.

Our spatial transcriptomics approach will also be useful to address other hypotheses regarding the tumor microenvironment, for instance whether close vicinity of (subpopulations of) dendritic cells with T cells is beneficial for patients, and whether T cells essential for anti-tumor response are located within cTIL, sTIL and/or elsewhere. This latter question is of major importance for a better selection of patients susceptible to respond to immunotherapy. Additionally, there is

FIGURE 4 Clonal expansion of intra-epithelial T cells as compared with matched stromal ones. (A) Estimation of the diversity of the immune repertoire (TCR and BCR) of intra-epithelial TIL, that is, located in TC core (cTIL), and matched stromal TIL (sTIL) among the seven FFPE TNBC samples. Repertoire diversity was estimated using Chao1 estimator. (B-C) Analysis of cTIL and sTIL TCR repertoires obtained from specific TCR sequencing of seven FF samples. Shannon entropy (B) reflects repertoires diversity while clonality (C) refers to evenness and clonal dominance. The number of TCR clones identified in each repertoire is indicated. P values were calculated with two-tailed paired T-tests. (D) Relative proportion of clonotypes with specific frequencies in cTIL vs sTIL from seven FF samples. (E) Venn diagrams show the overlap between cTIL and corresponding sTIL TCR repertoires for each FF sample. The number of clonotypes in each compartment as well as the cumulative frequency of shared clonotypes (ie, their relative contribution in each repertoires) for both cTIL (red) and sTIL (blue) repertoires are indicated. (F) Violin plots depict the distribution of clonotypes frequencies. Colored lines connect the top 10 most-clonally expanded TCRs from cTIL (blue and green) or sTIL (blue and red) repertoires in each repertoire.

increasing focus on models suggesting that different subtypes of T cells need to associate with different antigen presenting cells and stromal components in order to optimally support anti-tumor immune responses. Our approach will be helpful in addressing these questions and optimize future therapies.

AUTHOR CONTRIBUTIONS

The work reported in the paper has been performed by the authors, unless clearly specified in the text. Sana Intidhar Labidi-Galy and Petros Tsantoulis: supervision of the work. Lou Romanens, Stephan Ryser, Jean-Christophe Tille, Ketty Heimgartner-Hu, Killian Heimgartner, Jonathan S. Moore, Alexandre Harari, Raphael Genoet: generation of the data. Prasad Chaskar, Rachel Marcone, Raphael Genoet and Nicolas Liaudet: bioinformatic analysis. All authors: writing the manuscript.

ACKNOWLEDGEMENTS

Sana Intidhar Labidi-Galy is supported by funding from the Swiss National Science Foundation (Ambizione n° PZ00P3_173959), la Ligue Genevoise Contre le Cancer (grant n°1712), la Fondation pour la lutte contre le cancer et pour des recherches médico-biologiques and The Novartis Biomedical Research Foundation (#17C150). Petros Tsantoulis and Prasad Chaskar are supported by funding from La Ligue Genevoise Contre le Cancer. We thank Dr Mylene Doquier and Mr Didier Chollet from the platform of Genomics at the Faculty of Medicine, UNIGE, for their technical support. Open access funding provided by Universite de Geneve.

CONFLICT OF INTEREST STATEMENT

The University of Lausanne and the Ludwig Institute for Cancer Research have filed for patent protection on the TCR sequencing technology. Raphael Genoet is named as inventor on this patent. The other authors do not declare a conflict of interest.

DATA AVAILABILITY STATEMENT

All raw and processed RNA-sequencing data generated in this study have been submitted to the Array Express database under accession numbers E-MTAB-8760 and E-MTAB-11903. TCR-sequencing data is deposited at European Genome-Phenome Archive EGA repository under accession number EGAS00001007125. Other data that support the findings of this study are available from the corresponding author upon request.

ETHICS STATEMENT

The study was conducted in accordance with the declaration of Helsinki and the Swiss ethics Law HRA Art.34/HRO that authorizes further use of clinical samples without consent. The research protocol was approved by the ethics committee of Geneva (CCER: 2018-02333).

ORCID

Lou Romanens  <https://orcid.org/0000-0002-6454-0503>

Rachel Marcone  <https://orcid.org/0000-0002-5711-8435>

Jean-Christophe Tille  <https://orcid.org/0000-0002-2255-5918>

Nicolas Liaudet  <https://orcid.org/0000-0002-0749-5857>

Pierre-Yves Dietrich  <https://orcid.org/0000-0002-7375-6939>

Mauro Delorenzi  <https://orcid.org/0000-0001-7631-3263>

Petros Tsantoulis  <https://orcid.org/0000-0003-3613-6682>

Sana Intidhar Labidi-Galy  <https://orcid.org/0000-0002-0824-3475>

REFERENCES

- Hanahan D, Coussens LM. Accessories to the crime: functions of cells recruited to the tumor microenvironment. *Cancer Cell*. 2012;21(3):309-322. doi:10.1016/j.ccr.2012.02.022
- Balkwill FR, Capasso M, Hagemann T. The tumor microenvironment at a glance. *J Cell Sci*. 2012;125(Pt 23):5591-5596. doi:10.1242/jcs.116392
- Fridman WH, Zitvogel L, Sautes-Fridman C, et al. The immune contexture in cancer prognosis and treatment. *Nat Rev Clin Oncol*. 2017;14:717-734. doi:10.1038/nrclinonc.2017.101
- Loi S, Drubay D, Adams S, et al. Tumor-infiltrating lymphocytes and prognosis: a pooled individual patient analysis of early-stage triple-negative breast cancers. *J Clin Oncol*. 2019;37(7):559-569. doi:10.1200/JCO.18.01010
- Salgado R, Denkert C, Demaria S, et al. The evaluation of tumor-infiltrating lymphocytes (TILs) in breast cancer: recommendations by an International TILs Working Group 2014. *Ann Oncol*. 2015;26(2):259-271. doi:10.1093/annonc/mdu450
- Cabrita R, Lauss M, Sanna A, et al. Tertiary lymphoid structures improve immunotherapy and survival in melanoma. *Nature*. 2020;577(7791):561-565. doi:10.1038/s41586-019-1914-8
- Hegde PS, Karanikas V, Evers S. The where, the when, and the how of immune monitoring for cancer immunotherapies in the era of checkpoint inhibition. *Clin Cancer Res*. 2016;22(8):1865-1874. doi:10.1158/1078-0432.CCR-15-1507
- Simoni Y, Becht E, Fehlings M, et al. Bystander CD8(+) T cells are abundant and phenotypically distinct in human tumour infiltrates. *Nature*. 2018;557(7706):575-579. doi:10.1038/s41586-018-0130-2
- Joshi K, de Massy MR, Ismail M, et al. Spatial heterogeneity of the T cell receptor repertoire reflects the mutational landscape in lung cancer. *Nat Med*. 2019;25(10):1549-1559. doi:10.1038/s41591-019-0592-2
- Scheper W, Kelderman S, Fanchi LF, et al. Low and variable tumor reactivity of the intratumoral TCR repertoire in human cancers. *Nat Med*. 2019;25(1):89-94. doi:10.1038/s41591-018-0266-5
- Rizvi NA, Hellmann MD, Snyder A, et al. Cancer immunology. Mutational landscape determines sensitivity to PD-1 blockade in non-small cell lung cancer. *Science*. 2015;348(6230):124-128. doi:10.1126/science.aaa1348
- Schumacher TN, Schreiber RD. Neoantigens in cancer immunotherapy. *Science*. 2015;348(6230):69-74. doi:10.1126/science.aaa4971
- Yusko E, Vignali M, Wilson RK, et al. Association of tumor microenvironment T-cell repertoire and mutational load with clinical outcome after sequential checkpoint blockade in melanoma. *Cancer Immunol Res*. 2019;7(3):458-465. doi:10.1158/2326-6066.CIR-18-0226
- Zhang J, Ji Z, Caushi JX, et al. Compartmental analysis of T-cell clonal dynamics as a function of pathologic response to neoadjuvant PD-1 blockade in resectable non-small cell lung cancer. *Clin Cancer Res*. 2020;26(6):1327-1337. doi:10.1158/1078-0432.CCR-19-2931
- Gros A, Robbins PF, Yao X, et al. PD-1 identifies the patient-specific CD8(+) tumor-reactive repertoire infiltrating human tumors. *J Clin Invest*. 2014;124(5):2246-2259. doi:10.1172/JCI73639
- Elias KM, Tsantoulis P, Tille JC, et al. Primordial germ cells as a potential shared cell of origin for mucinous cystic neoplasms of the pancreas and mucinous ovarian tumors. *J Pathol*. 2018;246(4):459-469. doi:10.1002/path.5161

17. Labidi-Galy SI, Papp E, Hallberg D, et al. High grade serous ovarian carcinomas originate in the fallopian tube. *Nat Commun.* 2017;8(1):1093. doi:10.1038/s41467-017-00962-1
18. Gruosso T, Gigoux M, Manem VSK, et al. Spatially distinct tumor immune microenvironments stratify triple-negative breast cancers. *J Clin Invest.* 2019;129(4):1785-1800. doi:10.1172/JCI96313
19. Vincek V, Nassiri M, Knowles J, Nadjji M, Morales AR. Preservation of tissue RNA in normal saline. *Lab Invest.* 2003;83(1):137-138. doi:10.1097/O1.lab.0000047490.26282.cf
20. Amini P, Ettl J, Opitz L, Clementi E, Malbon A, Markkanen E. An optimised protocol for isolation of RNA from small sections of laser-capture microdissected FFPE tissue amenable for next-generation sequencing. *BMC Mol Biol.* 2017;18(1):22. doi:10.1186/s12867-017-0099-7
21. Espina V, Wulfkühle JD, Calvert VS, et al. Laser-capture microdissection. *Nat Protoc.* 2006;1(2):586-603. doi:10.1038/nprot.2006.85
22. Clement-Ziza M, Munnich A, Lyonnet S, et al. Stabilization of RNA during laser capture microdissection by performing experiments under argon atmosphere or using ethanol as a solvent in staining solutions. *RNA.* 2008;14(12):2698-2704. doi:10.1261/rna.1261708
23. Schuierer S, Carbone W, Knehr J, et al. A comprehensive assessment of RNA-seq protocols for degraded and low-quantity samples. *BMC Genomics.* 2017;18(1):442. doi:10.1186/s12864-017-3827-y
24. Cieslik M, Chugh R, Wu YM, et al. The use of exome capture RNA-seq for highly degraded RNA with application to clinical cancer sequencing. *Genome Res.* 2015;25(9):1372-1381. doi:10.1101/gr.189621.115
25. Priedigkeit N, Watters RJ, Lucas PC, et al. Exome-capture RNA sequencing of decade-old breast cancers and matched decalcified bone metastases. *JCI Insight.* 2017;2(17):e95703. doi:10.1172/jci.insight.95703
26. Rudloff U, Bhanot U, Gerald W, et al. Biobanking of human pancreas cancer tissue: impact of ex-vivo procurement times on RNA quality. *Ann Surg Oncol.* 2010;17(8):2229-2236. doi:10.1245/s10434-010-0959-6
27. Kufe DW. MUC1-C oncoprotein as a target in breast cancer: activation of signaling pathways and therapeutic approaches. *Oncogene.* 2013;32(9):1073-1081. doi:10.1038/onc.2012.158
28. Becht E, Giraldo NA, Lacroix L, et al. Estimating the population abundance of tissue-infiltrating immune and stromal cell populations using gene expression. *Genome Biol.* 2016;17(1):218. doi:10.1186/s13059-016-1070-5
29. Genolet R, Bobisse S, Chiffelle J, et al. TCR sequencing and cloning methods for repertoire analysis and isolation of tumor-reactive TCRs. *Cell Reports Methods.* 2023;3(4):100459. doi:10.1016/j.crmeth.2023.100459
30. Adams S, Gray RJ, Demaria S, et al. Prognostic value of tumor-infiltrating lymphocytes in triple-negative breast cancers from two phase III randomized adjuvant breast cancer trials: ECOG 2197 and ECOG 1199. *J Clin Oncol.* 2014;32(27):2959-2966. doi:10.1200/JCO.2013.55.0491
31. Egelston CA, Avalos C, Tu TY, et al. Resident memory CD8+ T cells within cancer islands mediate survival in breast cancer patients. *JCI Insight.* 2019;4(19):e130000. doi:10.1172/jci.insight.130000
32. Webb JR, Milne K, Nelson BH. PD-1 and CD103 are widely coexpressed on prognostically favorable intraepithelial CD8 T cells in human ovarian cancer. *Cancer Immunol Res.* 2015;3(8):926-935. doi:10.1158/2326-6066.CIR-14-0239
33. Webb JR, Milne K, Watson P, Leeuw RJ, Nelson BH. Tumor-infiltrating lymphocytes expressing the tissue resident memory marker CD103 are associated with increased survival in high-grade serous ovarian cancer. *Clin Cancer Res.* 2014;20(2):434-444. doi:10.1158/1078-0432.CCR-13-1877
34. Djenidi F, Adam J, Goubar A, et al. CD8+CD103+ tumor-infiltrating lymphocytes are tumor-specific tissue-resident memory T cells and a prognostic factor for survival in lung cancer patients. *J Immunol.* 2015;194(7):3475-3486. doi:10.4049/jimmunol.1402711
35. Meier SL, Satpathy AT, Wells DK. Bystander T cells in cancer immunology and therapy. *Nat Cancer.* 2022;3(2):143-155. doi:10.1038/s43018-022-00335-8
36. Loi S, Michiels S, Adams S, et al. The journey of tumor-infiltrating lymphocytes as a biomarker in breast cancer: clinical utility in an era of checkpoint inhibition. *Ann Oncol.* 2021;32:1236-1244. doi:10.1016/j.annonc.2021.07.007
37. Wall I, Boulat V, Shah A, et al. Leveraging the dynamic immune environment triad in patients with breast cancer: tumour, lymph node, and peripheral blood. *Cancers (Basel).* 2022;14(18):4505. doi:10.3390/cancers14184505
38. Schmid P, Cortes J, Dent R, et al. Event-free survival with Pembrolizumab in early triple-negative breast cancer. *N Engl J Med.* 2022;386(6):556-567. doi:10.1056/NEJMoa2112651
39. Cortes J, Rugo HS, Cescon DW, et al. Pembrolizumab plus chemotherapy in advanced triple-negative breast cancer. *N Engl J Med.* 2022;387(3):217-226. doi:10.1056/NEJMoa2202809

SUPPORTING INFORMATION

Additional supporting information can be found online in the Supporting Information section at the end of this article.

How to cite this article: Romanens L, Chaskar P, Marccone R, et al. Clonal expansion of intra-epithelial T cells in breast cancer revealed by spatial transcriptomics. *Int J Cancer.* 2023; 153(9):1568-1578. doi:10.1002/ijc.34620